Partitioned postseismic deformation associated with the 2009 Mw 6.3 L'Aquila earthquake surface rupture measured using a terrestrial laser scanner

GEOPHYSICAL RESEARCH LETTERS, VOL. 37, L10309, doi:10.1029/2010GL043099, 2010

Partitioned postseismic deformation associated with the 2009 Mw 6.3 L'Aquila earthquake surface rupture measured using a terrestrial laser scanner

M. Wilkinson,[1] K. J. W. McCaffrey,[1] G. Roberts,[2] P. A. Cowie,[3] R. J. Phillips,[4] Alessandro Maria Michetti,[5] E. Vittori,[6] L. Guerrieri,[6] A. M. Blumetti,[6] A. Bubeck,[7] A. Yates,[8] and G. Sileo[5]

Received 3 March 2010; revised 7 April 2010; accepted 16 April 2010; published 25 May 2010.

[1] Using 3D terrestrial laser scan (TLS) technology, we have recorded postseismic deformation on and adjacent to the surface rupture formed during the 6th April 2009 L'Aquila normal faulting earthquake (Mw 6.3). Using surface modeling techniques and repeated surveys 8–124 days after the earthquake, we have produced a 4D dataset of postseismic deformation across a 3 × 65 m area at high horizontal spatial resolution. We detected millimetre-scale movements partitioned between discrete surface rupture slip and development of a hangingwall syncline over 10's of meters. We interpret the results as the signal of shallow afterslip in the fault zone. We find 52% of the total postseismic hangingwall vertical motion occurs as deformation within 30 m of the surface rupture. The total postseismic vertical motions are approximately 50% that of the coseismic. We highlight the importance of quantifying partitioned postseismic contributions when applying empirical slip-magnitude datasets to infer palaeoearthquake magnitudes. **Citation:** Wilkinson, M., et al. (2010), Partitioned postseismic deformation associated with the 2009 Mw 6.3 L'Aquila earthquake surface rupture measured using a terrestrial laser scanner, *Geophys. Res. Lett.*, *37*, L10309, doi:10.1029/2010GL043099.

1. Introduction

[2] Earthquakes produce coseismic motions that may amplify during the weeks after the mainshock. We report the novel use of a Terrestrial Laser Scanner (TLS) to monitor postseismic ground surface deformation following the 6th April 2009, M_w 6.3 earthquake, which struck L'Aquila in the Abruzzo region, Italy. Field observations [*Falcucci et al.*, 2009] in the days after the earthquake identified a discontinuous surface rupture ~12 km in length, with discontinuous ruptures over a distance of 2 km along the Paganica fault, situated northeast of Paganica (Figure 1). InSAR and body-wave seismology studies identified the earthquake slip plane as a SW-dipping normal fault with ~0.6–0.8 m coseismic slip at depth, propagating to the surface on the Paganica fault [*Atzori et al.*, 2009; *Walters et al.*, 2009]. The Paganica rupture, as observed in the field has normal sense displacement with a consistent downthrow along its length towards 218° ± 5° constrained by opening directions across ground cracks. Observed coseismic throw across localised cracks and ruptures ranged from 0.7–15.0 cm [*Galli et al.*, 2009; *Falcucci et al.*, 2009; *Emergeo Working Group*, 2010]. Observations with InSAR on Envisat tracks predicted "surface ruptures of ~10 cm" [*Walters et al.*, 2009]. Postseismic afterslip for the L'Aquila event has been inferred using a laser strain meter system located 20 km NE of the epicentre [*Amoruso and Crescentini*, 2009]. Also field observations documented the widening of ground cracks and increased surface offsets along the surface rupture observed over two months after the earthquake [*Galli et al.*, 2009; *Boncio et al.*, 2010]. Our study monitored the postseismic ground surface deformation of a concrete road (Site ID. PAG, 13.471450°E 42.362631°N). The road is perpendicular to the strike of the Paganica fault, across which a sharp surface rupture had formed. This section of the surface rupture is close to the centre of the overall trace with measured vertical offset of ~7.5 cm when we first visited the site on the 14th April, 8 days after the earthquake (Figure 1).

2. Method

[3] Terrestrial laser scanning is a relatively new form of ground based remote sensing. The time of flight of an emitted laser and its reflected returning counterpart are used to calculate the range between a tripod-mounted laser scanner and the ground surface. By incrementally adjusting the direction in vertical and horizontal steps, the scanner is able to sample reflections from regularly spaced areas of the ground surface within the line of sight of the scanner. For each ground reflection a unique point in 3D space is calculated, with many ground reflections populating a point cloud dataset. At study site PAG, using a Riegl LMS-z420i laser scanner with single point precision of 8 mm at 50 m range (Riegl LMS-420i datasheet, available at http://riegl.com/uploads/tx_pxpriegldownloads/10_DataSheet_Z420i_18-03-2010.pdf), point clouds of ~2.5 million individual points spaced between 4–10 mm apart were acquired, defining 195 m^2 of the road surface. A network of five reflector positions was

[1]Department of Earth Sciences, Durham University, Durham, U.K.
[2]School of Earth Sciences, Birkbeck College, University of London, London, U.K.
[3]School of Geosciences, University of Edinburgh, Edinburgh, U.K.
[4]Institute of Geophysics and Tectonics, University of Leeds, Leeds, U.K.
[5]Dipartmento di Scienze Chimiche e Ambientale, Università dell'Insubria, Como, Italy.
[6]Geological Survey of Italy, High Institute for the Environmental Protection and Research, Rome, Italy.
[7]Geospatial Research Ltd., Department of Earth Sciences, Durham University, Durham, U.K.
[8]Department of Earth Sciences, Uppsala University, Uppsala, Sweden.

0094-8276/10/2010GL043099

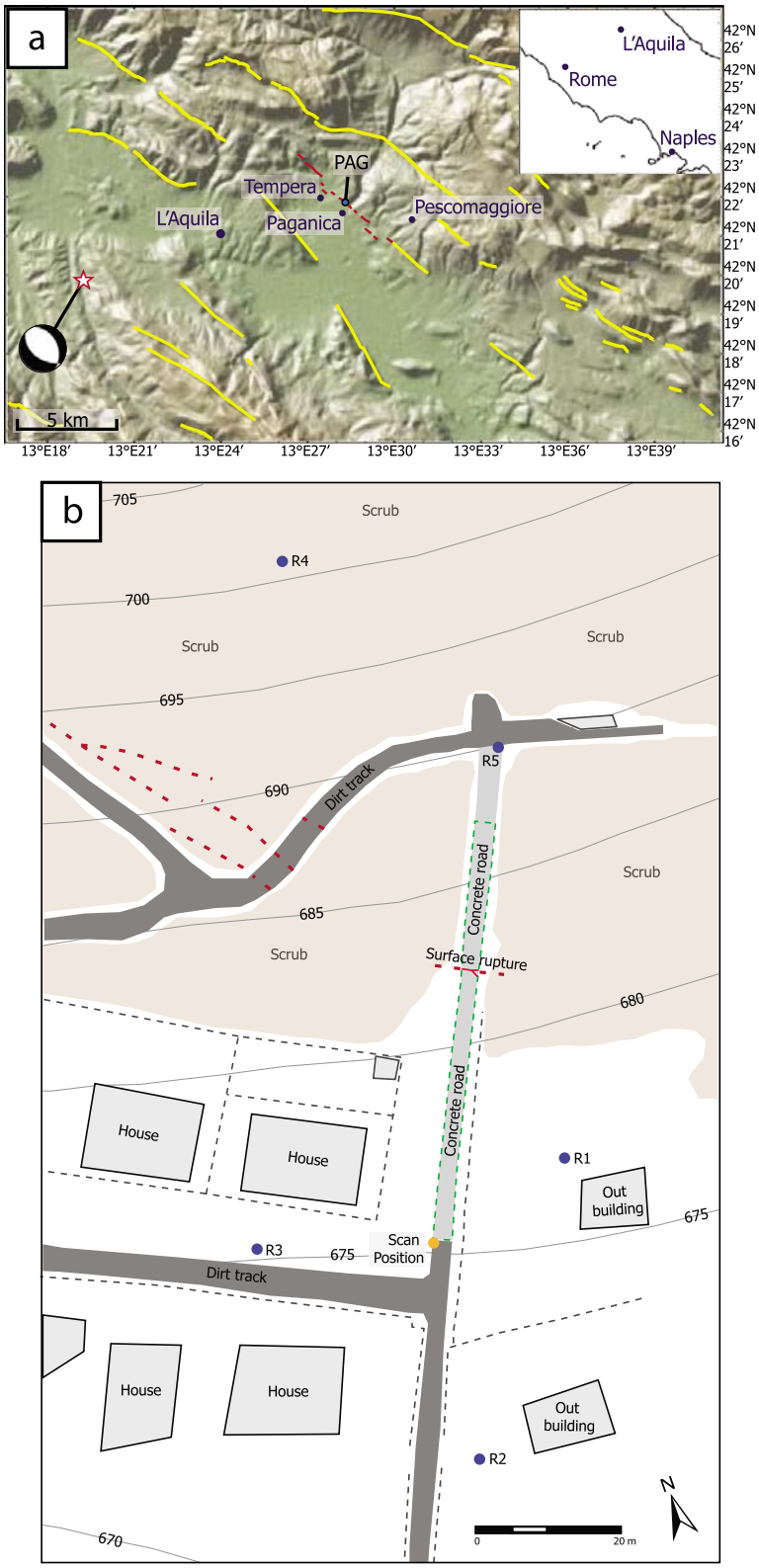

Figure 1. (a) Interpreted active normal faults of the Abruzzo region with the L'Aquila earthquake surface ruptures along the Paganica fault shown in red (adapted from *Roberts* [2008], *Falcucci et al.* [2009], *Michetti et al.* [2000], and ISPRA (Geological effects induced by the L'Aquila earthquake (6 April 2009, MI = 5.8) on the natural environment: Preliminary report, 2009, available at http://www.apat.gov.it/site/en-GB/Projects/INQUA_Scale/Documents/). The star south west of L'Aquila marks the hypocentre of the 2009 main shock with Quick gCMT focal mechanism attached (Strike 127°, Dip 50°, Rake −109°). (b) Site map of PAG showing the modeled dataset boundary inside the green dashed line and the location of the scan position and five reflectors. The discontinuous nature of the surface rupture outside the dataset boundary is shown by red dashed lines.

Table 1. Survey dates and measurements of rupture throw, syncline subsidence, combined rupture throw and syncline subsidence and line of sight extension between reflectors for each of the TLS datasets (PAG2-PAG7), relative to the first PAG1 datum

Date	Dataset ID	Days since earthquake	Rupture throw since 14/04/09 (mm)	Syncline subsidence since 14/04/09 (mm)	Combined rupture throw and syncline subsidence since 14/04/09 (mm)	Line of sight extension between reflectors since 14/04/09 (mm)
14/04/09	PAG 1	8	-	-	-	-
17/04/09	PAG 2	11	2.2	11.6	13.8	11.4
11/05/09	PAG 3	35	3.9	19.5	23.4	15.9
15/05/09	PAG 4	39	4.1	19.4	23.5	9.3
19/05/09	PAG 5	43	5.2	17.3	22.5	16.4
24/05/09	PAG 6	48	8.3	16.2	24.5	17.2
08/08/09	PAG 7	124	13.4	14.3	27.7	21.8

created, including sites 20 m into the footwall and 40 m into the hangingwall (Figure 1). Repeat datasets were obtained on seven occasions between 8 and 124 days after the main earthquake (Table 1). The reflectors were used as control points to position the point cloud datasets into a footwall-static reference frame relative to the day 8 dataset. A point cloud acquired for any scanned surface shows a Gaussian distribution of errors about the mean, which represents a close approximation to the real surface. A representative road surface for each of the seven TLS datasets for PAG was created using the discrete smooth interpolation (DSI) method [*Mallet*, 1992]. The DSI operates by creating a preliminary meshed surface with triangle vertices spaced 10 × 10 cm. Each of the triangle vertices are then translated to a location which represents the mean of the local surrounding points within the point cloud dataset (see Figure S1 for a workflow of the method).[1] The high density of our point clouds allowed us to detect minimum vertical differences between modeled surfaces of 1.5–5.7 mm, dependent on the part of the surface being compared, with 95% confidence (based on the 2σ variation in the moving point average for triangle vertices, window size 250 points, used to create the cross sectional plots in Figure 2b). Comparison of the vertical difference between the initial hangingwall surface and each subsequent surface allowed quantification of the near field postseismic hangingwall deformation relative to day 8 (Figure 2). The 5-point reflector network also enabled us to measure horizontal extension by comparing the average change in horizontal distance between reflectors paired across the fault relative to their horizontal distance at day 8.

3. Data and Comparison With Existing Afterslip Models

[4] Our datasets allowed us to precisely measure the relative vertical movement for points on the 65 × 3 m road surface (Figure 2). Two discrete styles of surface motion were observed. Firstly, throw on the rupture increased by 13.4 mm ± 2.6 mm between day 8 and day 124. Secondly, in addition to throw on the rupture, a further 14.3 mm ± 2.3 mm of vertical offset was measured, associated with growth of a warp or hangingwall syncline between day 8 and 124, originating from 7 m into the hangingwall. The syncline increased in width from 20 metres between days 8 and 15, to >30 m by day 124. The maximum vertical offset which developed between 8 and 124 days after the earthquake for the combined rupture and syncline was 27.7 mm ± 2.3 mm. We note that 14.3 mm of this value (52%) would have been missed if the syncline had not been recognised and measured. Horizontal extension measured by averaging the change in distance between reflectors paired across the rupture totalled 21.8 mm ± 5.0 mm. Measurements of extension over intermediate time periods are similar to the equivalent combined rupture and syncline vertical motions (Figure 3). The postseismic displacements recorded at GPS stations close to our PAG survey site [*Cheloni et al.*, 2010] are in broad agreement with the vertical motions we observe.

[5] We compare our measured datasets with previously published theoretical and empirical models that describe measured afterslip from rupture studies following previous earthquakes [*Bucknam et al.*, 1978; *Williams and Magistrale*, 1989; *Marone et al.*, 1991] (Figures 3 and 4). These models have not been optimised to fit our data; they have been plotted relative to day 8, our first observation, using published parameters defined from measured afterslip following previous earthquakes [*Bucknam et al.*, 1978; *Sharp et al.*, 1989; *Williams and Magistrale*, 1989].

4. Discussion

[6] The data for rupture throw, not including syncline subsidence, are indicative of afterslip, showing broad agreement with previously published afterslip models with correlation coefficients ranging from 0.9149–0.9318 (Figure 3). To estimate how much afterslip occurred on the rupture before our measurements began, we utilise field observations 500 m–1500 m SE from our site, PAG by *Boncio et al.* [2010]. They document the widening of a ground fracture by 30–50 mm between the 6th and 25th April and the vertical development of a hangingwall flexure by 25 mm between the 6th April and 19th May; we estimate 15 mm of this vertical motion developed between 6th–14th April. We measured 75 mm of offset across the rupture on the 14th April. If the observations of *Boncio et al.* [2010] apply to our site, we suggest that ~15 mm of this measurement was produced by postseismic deformation on the rupture prior to 14th April. By adding 15 mm to our observation of 13.4 mm of rupture throw observed between 14th April and 8th August, we estimate the total measured afterslip on the rupture since 6th April to be ~30 mm, in broad agreement with the previously published models. This estimate suggests afterslip at PAG is around 50% of the mostly coseismic offset totalling 75 mm observed across the rupture on the 14th April. However, if the postseismic deformation associated with syncline growth are added to those of rupture throw, the models describe such combined motions with lower

[1] Auxiliary materials are available in the HTML. doi:10.1029/2010GL043099.

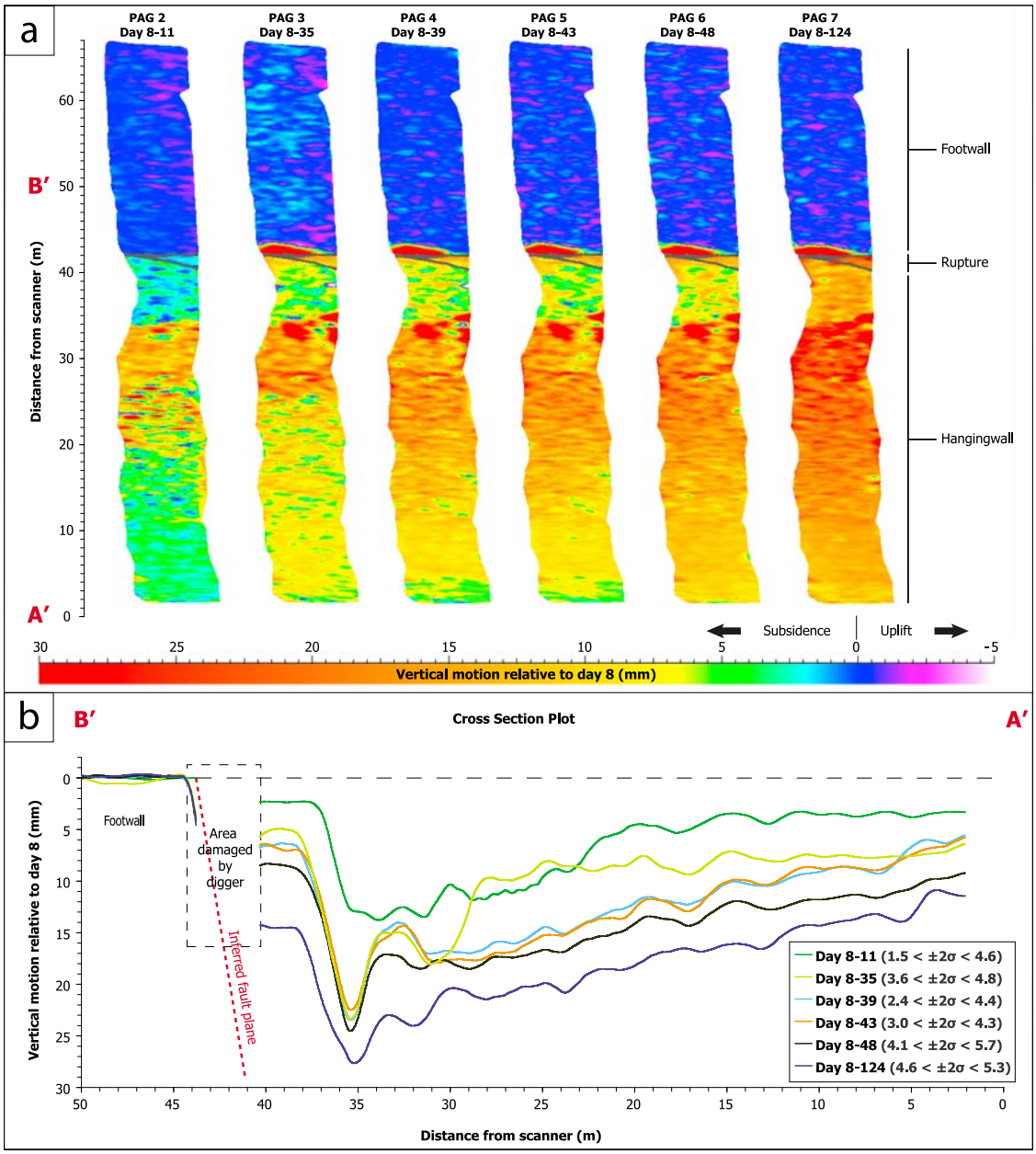

Figure 2. (a) Color map plots showing vertical motion values (mm) in a footwall static reference frame in 3D space for TLS datasets PAG2–PAG7, relative to the first scanned dataset PAG1 (8 days after the earthquake). A time lapse animation of the vertical motions is available in Movie S1. (b) Cross sectional plot taken perpendicular to the main strike of the rupture between A′ and B′. Each plot was calculated using a moving point average with window size 250 points (representing 3 m width × 0.7 m distance along the road), using the vertical motion values from each of the colour map plots in Figure 2a. The boxed zone highlights an area of damage (breaking off of the footwall) the surface rupture received between days 11 and 35 attributed to a digger being driven over it. The similarity of the deformation observed along the rest of the road before and after the digger damage shows that the immediate 2–3 m of footwall was the only part of the road which was vulnerable and subsequently damaged. $\pm 2\sigma$ bounds represent the range of certainty in vertical motion for each cross sectional plot which changes along section due to variations in the smoothness of the road.

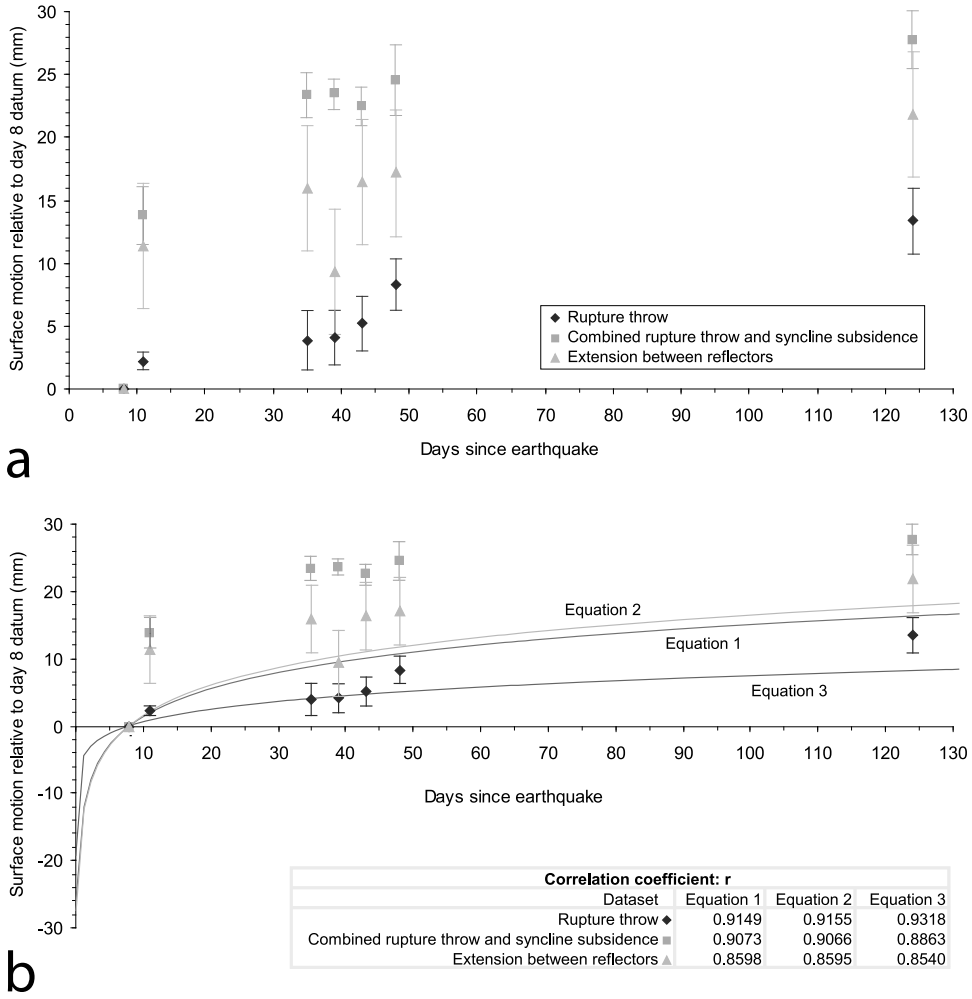

Figure 3. (a) Surface motions for the six TLS datasets (PAG2–PAG7), relative to the initial TLS dataset PAG1, 8 days following the earthquake (Table 1) plotted against time since the earthquake. Error bars represent 2σ (95%) certainty. (b) Graphical comparison of published theoretical and empirical models for afterslip (Equations 1, 2 and 3 in Figure 4) to our datasets, together with their correlation coefficients.

correlation coefficients 0.8863–0.9073, largely because of the relatively rapid syncline subsidence between days 8–11. Between days 8–124, the rate and magnitude of syncline subsidence were comparable to and at times exceeded that of the rupture afterslip, with the combined rupture afterslip and syncline subsidence being approximately twice that of the rupture afterslip at day 124. The similarity in magnitude of the combined rupture throw and syncline subsidence in relation to the data for horizontal extension suggests that hangingwall deformation responsible for syncline growth formed a major component of the postseismic extension at PAG.

[7] Numerous studies suggest the growth of hangingwall synclines are common during normal faulting earthquakes. Hangingwall synclines are observed at many palaeoseismic sites within the Italian Apennines [*D'Addezio et al.*, 1996; *Pantosti et al.*, 1996; *Galli et al.*, 2002; *Galli et al.*, 2008]. Also, surface motions described as 'uplift of the footwall and a warp-like hangingwall subsidence (folding)' were recorded during a study of afterslip on the surface rupture of the 1995 Egion earthquake [*Koukouvelas and Doutsos*, 1996]. Indeed, we have observed progressive development of hangingwall synclines, with similar subsidence in preliminary processing of TLS datasets spanning equivalent time periods at two other sites along the Paganica surface rupture (Figures S2 and S3).

[8] The localised nature of surface motions at PAG produced several centimetres of slip across the rupture that was visible with the naked eye. However, we note that the vertical motions associated with syncline growth would have been missed without the use of TLS, as they were too subtle to observe with the naked eye alone, and no pre-earthquake datum existed in the form of a precise topographic map. This is important because such subtle subsidence associated with hangingwall folding accounts for 52% of the total vertical postseismic deformation. Such deformation may be un-accounted for within empirical slip-magnitude relationships, especially for smaller earthquakes [e.g., *Wells and Coppersmith*, 1994]. If this is the case, we note that in our study, the inclusion of hangingwall deformation would have doubled the surface offset for the given earthquake magnitude, if the total subsidence had not been attributed to a combination of postseismic and coseismic deformation. In palaeoseismic studies such slip-magnitude datasets are used to

$D = a + b\log T$ (1)[1]	$U^P = U_C^S + \alpha' \ln\left[\left(\frac{\beta'}{\alpha'}\right)t + 1\right]$ (2)[2]	$D = at^b$ (3)[3]
[1]Model 1: Equation defined by least-squares regression of observed displacement data on logarithm of time from the 1976 Guatemala earthquake [*Buckham et al.*, 1978]. D = modeled displacement (mm) a = coseismic rupture offset (mm) b = gradient of best fit line through the data plotted as logarithm of time T = time since earthquake (days)	[2]Model 2: Two variable version of a closed-form solution for afterslip [*Marone et al.*, 1991, after *Scholtz*, 1990] modified to accommodate coseismic measurements, and used to model 1987 Superstition Hills afterslip data [*Sharp et al.*, 1989]. U_P = modeled displacement (mm) U^S_c = coseismic rupture offset (mm) α' = a parameter (mm) defining the friction rate parameter divided by spring stiffness, analogous to the thickness of the velocity strengthening region, the former obtained from best fit to data plotted as logarithm of time β' = coseismic slip velocity in the velocity strengthening region (mm/day)	[3]Model 3: Slip decay model [*Williams and Magistrale*, 1989] describing displacement data from the 1987 Superstition Hills earthquake sites 2M, 2T and 2U. D = modeled displacement (mm) a = coseismic rupture offset (mm) b = decay rate parameter t = time since earthquake (days)

a (mm)	b	U^S_c (mm)	α'	β'	a (mm)	b
0 (replacement of 50.9 as there is no coseismic component to be compared in our dataset)	13.9	0 (replacement of 237.1 as there is no coseismic component to be compared in our dataset)	65.69	518.1	14.6	0.131
Parameters calculated from data of the 1976 Guatemala earthquake, Zacapa site.		Parameters calculated from data of the 1987 Superstition Hills Earthquake site 2T [*Sharp et al.*, 1989].			Parameters calculated from data of the 1987 Superstition Hills Earthquake, Site 2T.	

Figure 4. Theoretical and empirical afterslip models with parameters obtained from afterslip datasets of previous earthquakes.

estimate palaeoearthquake magnitudes from measured offsets [*Bakun et al.*, 2005; *Vigny et al.*, 2005; *Ryder et al.*, 2007]. Uncertainty in the surface offset for a given magnitude within the slip-magnitude datasets will lead to uncertainty in the palaeoearthquake magnitude for a given offset. Routine TLS surveying permits hangingwall synclines and other off-fault deformation to be quantified and distinguished from rupture slip.

[9] **Acknowledgments.** Funded by NERC grants NE/H003266/1 and NE/E016545/1 and Durham University Doctoral Fellowship (M. Wilkinson). We thank N. De Paola for assistance in the field M. Allen for comments on an earlier draft and D. Stevenson and G. Wilkinson for maintaining computing support. Meng Wei and an anonymous reviewer are thanked for their constructive comments.

References

Amoruso, A., and L. Crescentini (2009), Slow diffusive fault slip propagation following the 6 April 2009 L'Aquila earthquake, Italy, *Geophys. Res. Lett.*, *36*, L24306, doi:10.1029/2009GL041503.

Atzori, S., I. Hunstad, M. Chini, S. Salvi, C. Tolomei, C. Bignami, S. Stramondo, E. Trasatti, A. Antonioli, and E. Boschi (2009), Finite fault inversion of DInSAR coseismic displacement of the 2009 L'Aquila earthquake (central Italy), *Geophys. Res. Lett.*, *36*, L15305, doi:10.1029/2009GL039293.

Bakun, W. H., et al. (2005), Implications for prediction and hazard assessment from the 2004 Parkfield earthquake, *Nature*, *437*, 969–974, doi:10.1038/nature04067.

Boncio, P., A. Pizzi, F. Brozzetti, G. Pomposo, G. Lavecchia, D. Di Naccio, and F. Ferrarini (2010), Coseismic ground deformation of the 6 April 2009 L'Aquila earthquake (central Italy, M_w6.3), *Geophys. Res. Lett.*, *37*, L06308, doi:10.1029/2010GL042807.

Bucknam, R. C., G. Plafker, and R. V. Sharp (1978), Fault movement (afterslip) following the Guatemala earthquake of February 4, 1976, *Geology*, *6*, 170–173, doi:10.1130/0091-7613(1978)6<170:FMAFTG>2.0.CO;2.

Cheloni, D., et al. (2010), Coseismic and initial postseismic slip of the 2009 Mw 6.3 L'Aquila earthquake, Italy, from GPS measurements, *Geophys. J. Int.*, in press.

D'Addezio, G., D. Pantosti, and P. M. De Martini (1996), Palaeoseismologic and geomorphic investigations along the middle portion of the Ovindoli-Pezza Fault (Central Italy), *Ann. Geofis.*, *39*, 663–675.

Emergeo Working Group (2010), Evidence for surface rupture associated with the Mw 6.3 L'Aquila earthquake sequence of April 2009 (central Italy), *Terra Nova*, *22*, 43–51, doi:10.1111/j.1365-3121.2009.00915.x.

Falcucci, E., et al. (2009), The Paganica Fault and Surface Coseismic Ruptures Caused by the 6 April 2009 Earthquake (L'Aquila, Central Italy), *Seismol. Res. Lett.*, *80*, 940–950, doi:10.1785/gssrl.80.6.940.

Galli, P., F. Galadini, M. Moro, and C. Giraudi (2002), New palaeoseismological data from the Gran Sasso d'Italia area (cental Apennines), *Geophys. Res. Lett.*, *29*(7), 1134, doi:10.1029/2001GL013292.

Galli, P., F. Galadini, and D. Pantosti (2008), Twenty years of Palaeoseismology in Italy, *Earth Sci. Rev.*, *88*, 89–117, doi:10.1016/j.earscirev.2008.01.001.

Galli, P., et al. (2009), April 6, 2009 L'Aquila earthquake; macroseismic survey, surficial effects and seismotectonic implications, *Ital. J. Quat. Sci.*, *22*, 235–246.

Koukouvelas, I. K., and T. T. Doutsos (1996), Implications of structural segmentation during earthquakes: the 1995 Egion Earthquake, Gulf of Corinth, Greece, *J. Struct. Geol.*, *18*, 1381–1388, doi:10.1016/S0191-8141(96)00071-5.

Mallet, J. L. (1992), GOCAD: A computer aided design program for geological applications, in *Three Dimensional Modeling With Geoscientific Information Systems*, edited by A. K. Turner, pp. 123–141, Kluwer, Netherlands.

Marone, C. J., S. H. Scholtz, and R. Bilham (1991), On the mechanics of Earthquake Afterslip, *J. Geophys. Res.*, *96*, 8441–8452, doi:10.1029/91JB00275.

Michetti, A. M., L. Serva, and E. Vittori (2000), Italy hazard from Capable Faulting, a database of active capable faults of the Italian onshore territory [CD-ROM], report, Agenzia Nazionale Protezione Ambiente, Rome.

Pantosti, D., G. D'Addezio, and F. R. Cinti (1996), Palaeoseismicity of the Ovindoli-Pezza fault, central Apennines, Italy: A history including a large, previously unrecorded earthquake in the Middle Ages (860–1300 A.D.), *J. Geophys. Res.*, *101*, 5937–5959, doi:10.1029/95JB03213.

Roberts, G. P. (2008), Visualisation of active normal fault scarps in the Apennines, Italy: A key to assessment of tectonic strain release and earth-

quake rupture, in *Google Earth Science*, edited by D. De Paor, *J. Virtual Explorer*, *30*(4).

Ryder, I., P. Parsons, T. J. Wright, and G. J. Funning (2007), Post-seismic motion following the 1997 Manyi (Tibet) earthquake: InSAR observations and modeling, *Geophys. J. Int.*, *169*, 1009–1027, doi:10.1111/j.1365-246X.2006.03312.x.

Scholz, C. H. (1990), *The Mechanics of Earthquakes and Faulting*, Cambridge Univ. Press, New York.

Sharp, R. V., et al. (1989), Surface faulting along the Superstition Hills fault zone and nearby faults associated with the earthquakes of 24 November 1987, *Bull. Seismol. Soc. Am.*, *79*, 252–281.

Vigny, C., et al. (2005), Insight into the 2004 Sumatra–Andaman earthquake from GPS measurements in southeast Asia, *Nature*, *436*, 201–206, doi:10.1038/nature03937.

Walters, R. J., J. R. Elliott, N. D'Agostino, P. C. England, I. Hunstad, J. A. Jackson, B. Parsons, R. J. Phillips, and G. Roberts (2009), The 2009 L'Aquila earthquake (central Italy): A source mechanism and implications for seismic hazard, *Geophys. Res. Lett.*, *36*, L17312, doi:10.1029/2009GL039337.

Wells, D. L., and K. J. Coppersmith (1994), New empirical relationships among magnitude, rupture length, rupture width, rupture area and surface displacement, *Bull. Seismol. Soc. Am.*, *84*, 974–1002.

Williams, P. L., and H. W. Magistrale (1989), Slip along the Superstition Hills fault associated with the 24 November 1987 Superstition Hills, California, Earthquake, *Bull. Seismol. Soc. Am.*, *79*, 390–410.

A. M. Blumetti, L. Guerrieri, and E. Vittori, Geological Survey of Italy, High Institute for the Environmental Protection and Research, Via Curtatone, 3, I-00185 Roma, Italy.

A. Bubeck, Geospatial Research Ltd., Department of Earth Sciences, Durham University, Durham DH1 3LE, UK.

P. A. Cowie, School of Geosciences, University of Edinburgh, Drummond Street, Edinburgh EH8 9XP, UK.

K. J. W. McCaffrey and M. Wilkinson, Department of Earth Sciences, South Road, Durham University, Durham DH1 3LE, UK. (maxwell.wilkinson@durham.ac.uk)

A. M. Michetti and G. Sileo, Dipartmento di Scienze Chimiche e Ambientale, Università dell'Insubria, Via Valleggio 11, I-22100, Como, Italy.

R. J. Phillips, Institute of Geophysics and Tectonics, University of Leeds, Leeds LS2 9JT, UK.

G. Roberts, School of Earth Sciences, Birkbeck College, University of London, Malet Street, London WC1E 7HX, UK.

A. Yates, Department of Earth Sciences, Uppsala University, Villavägen 16, SE-75236 Uppsala, Sweden.